Magneto-mechanical actuation of ferromagnetic shape memory alloy/epoxy composites

☆http://dx.doi.org/10.1016/j.compscitech.2015.04.009

Susanne Glock, Luis P. Canal, Carolina M. Grize, Véronique Michaud*

Laboratory for Polymer and Composite Technology (LTC), Ecole Polytechnique Fédérale de Lausanne (EPFL), CH-1015 Lausanne, Switzerland

Abstract

Ferromagnetic shape memory alloys (MSMA) exhibit magnetic field- and stress-induced twinning when processed into single crystals, but are brittle and difficult to shape. Embedding slender single crystalline MSMA elements into a polymer matrix can thus provide composites with adjustable magnetic strain actuation behavior. Ni-Mn-Ga single crystalline rods were characterized for their magneto-mechanical behavior and embedded in two different types of epoxy matrices with different volumetric fractions. The magnetic actuation of the composites was measured and shown to depend on the Ni-Mn-Ga volumetric fraction and the matrix stiffness. This behavior was well predicted by finite element simulations of the composite using a simple material model for the strain of the MSMA as a function of the magnetic field and applied stresses. Guidelines for composite behavior prediction could thus be proposed.

Keywords: A. Smart materials, A. Functional composites, B. Magnetic properties, C. Finite element analysis (FEA), Magnetic actuation

*Corresponding author. Tel.: +41 21 693 49 23; fax: +41 21 693 58 80
Email address: veronique.michaud@epfl.ch (Véronique Michaud)

1. Introduction

Thermal shape memory alloys (TSMA) have found numerous applications over the last thirty years, in medicine, dentistry, robotics, etc [1], mostly owing to their superelastic properties in the austenitic phase. The actuating capacities of TSMA, resulting from the shape memory effect of these alloys, are also of interest for practical applications requiring large strains and recovery stresses but they are restricted to low frequencies (≤ 1 Hz), as a consequence of the relatively slow process of thermally induced martensite to austenite phase transformation [2]. Ferromagnetic shape memory alloys (MSMA) are a subset of the TSMA that show deformations up to 10% and 20 % in their martensitic state, upon the application of an external magnetic field or mechanical load, respectively [3]. This response is caused by the reorientation of twins in the tetragonal or pseudo-tetragonal martensite phase. Since twinning is a very fast process, high actuation frequencies of up to 2 kHz can be reached, and new applications can be envisaged [4, 5, 6]. Grain boundaries, however, increase the twinning stress, hinder twinning and prevent the magnetic field induced actuation. Thus, applications requiring high strain and actuation frequency have been up to now limited to expensive and brittle single crystals. A current research goal is to produce single crystalline powders and fibers of Ni-Mn-Ga with grains as large as the fiber diameter that exhibit considerable magnetic activation [7, 8, 9, 10, 11]. These elements can then be embedded in a polymer matrix to form a composite structure, easily shaped and suitable for applications with tailored magnetic actuation behavior. So far, mostly powder composites have been produced [4, 12, 13] and have demonstrated increased damping, but very little Magnetic Field Induced Strain (MFIS), of less than 0.1% [14, 15]. Gans et al. investigated the use of single crystal rods and showed promising actuation results, which they modeled with a simple analytical isostrain model [16] to evaluate the influence of matrix stiffness and MSMA volume fraction on the magnetic actuation of continuous MSMA elements embedded in a polymer matrix.

The deformation of composite materials is now generally predicted by computational simulations, which rely on the use of adequate constitutive models for each phase [17, 18]. Thus, numerical simulations of MSMA composites should incorporate the mechanical properties of the matrix, as well as the magneto-mechanical behavior observed in the MSMA. Moreover, the constitutive laws of the MSMA should be obtained with a minimal number of experimental determinations that correspond to their loading state in the composite.

Several phenomenological models are available, which describe their thermodynamic state by means of internal energy functions with mechanical and magnetic variables that need to be minimized [19, 20, 21]. These models have

shown accurate predictions of the experimental MFIS and magnetization curves in MSMA [22, 23, 24], and have been incorporated in 3D finite element models to reproduce the magneto-mechanical material response of the bulk MSMA under different fields and stresses [25, 26, 27]. However, these models require the experimental determination of many variables, and are generally developed to capture hysteretic or structural effects in the bulk material as a function of its composition and state.

In the present work, we propose to investigate the magneto-mechanical behavior of Ni-Mn-Ga single crystal rods embedded into epoxy matrices, experimentally and numerically. For this, Ni-Mn-Ga single crystal-epoxy matrix composites with different Ni-Mn-Ga volumetric fraction and matrix stiffness have been processed and investigated for their magnetic actuation behavior. To simulate the magneto-mechanical behavior of the single crystals at the macroscale, a simple three-dimensional phenomenological material model was proposed and implemented for FE analysis. This model relies on the identification of a stress-strain compression curve, and a stress-magnetic field curve for the MSMA rods, which were trained to exhibit only 2 types of variants. The mechanical response, including the pseudo-elastic behavior produced by the twining microstructure, was described using the formalism of computational plasticity. This formalism has been frequently used to simulate the pseudo-elastic behavior of SMA [28, 29, 30]. Then, the magnetic filed induced response was described from a fit of the stress-magnetic field response of the constrained single crystal. Finally, this material model was applied to predict the actuation behavior of single crystal composites under various mechanical and magnetic loading cases.

2. Materials and experimental techniques

The Ni-Mn-Ga rods used in this work were produced by Adaptamat, Finland, and had a 10M structure. They were delivered with a stabilizing surface treatment and a dimension of $20\times1\times1$ mm^3. To guarantee maximum elongation along the long sample axis, the crystals were cut by Adaptamat so as to keep their faces parallel to the {100} faces of the high temperature, austenitic phase. In addition, a training of the crystals resulted in an activation of only one out of the three possible twinning planes {101}, {011} and {110}. Thus, the single crystals could only transform between two different twin variants, variant 1 and variant 2 in Fig. 1, and the twinning strain upon magnetic and mechanical activation took place, as shown in Fig. 2, just in the directions x and y [20]. All rods were cut with a wire saw to obtain about 10 mm long samples.

Two epoxy systems of low modulus were selected: LME 10435 (resin)/LME 10436 (hardener) from Huntsman with a mix ratio of 100:123 by weight and

SR 8150 (resin)/SD 815 B1 (hardener) from Sicomin with a mix ratio of 100:16 by weight. Four model composite specimens each containing four Ni-Mn-Ga single crystalline rods embedded in the epoxy matrix were manufactured to investigate the magnetic actuation behavior of MSMA composites, with two different Ni-Mn-Ga volume fractions (13 and 34 vol.%), as shown in Fig. 3, and the two different matrices. Epoxy was cast into silicon molds containing the rods. In order to maintain the positions of the rods during casting, the procedure was as follows: the rods were first glued with a drop of epoxy on a cuboid of already cured epoxy using a geometrical device that allowed to position the rods according to the desired volume fraction with a constant intra-rod distance equal to the distance between rod and sample edge. After curing the drops for 2 days at room temperature, the positioning device was removed. To avoid a thermal reverse martensitic phase transformation of the Ni-Mn-Ga rods which takes place at about 53 °C, the composite samples were cured at room temperature during 21 days.

The magneto-mechanical behavior of the single crystalline Ni-Mn-Ga rods and of the four Ni-Mn-Ga composites was characterised with the experimental set-up shown in Fig. 4. It consisted of micrometer screws to measure the displacement of the sample, of a 500 N piezoelectric high-sensitivity tensile and compression force sensor 9217A from Kistler, Switzerland, and of a glass extension bar to ensure that the measurement of the load is not influenced by the magnetic field. Turning the micrometer screws allowed to lower/raise the extension bar. The magnetic field of maximum 1.2 T for this configuration was generated by a dipole electromagnet 5403 from GMW Associates, US, and measured by a MagVector 3D Hall sensor of Sensima technology SA, Switzerland. Magnetic field and force were simultaneously recorded using a LabVIEW program.

The stress-strain behavior of the Ni-Mn-Ga single crystals was determined through uniaxial compression tests. Prior to each test, the single crystals were magnetized in a homogeneous magnetic field of 1.2 T perpendicular to the long sample axis in order to ensure a detwinned, long initial sample state. The samples were compressed in steps of 12.5 μm up to a compression of 50 μm and in steps of 25 μm up to a compression corresponding to the detwinned, short sample state and unloaded in steps of 12.5 μm.

The magnetic field induced stress was measured on a Ni-Mn-Ga single crystal in its detwinned, short state. To obtain this state, the sample was magnetized along the long sample axis in a magnetic field of 1.2 T. During the test, the initial position of the extension rod, just touching the sample, was kept constant while the magnetic field perpendicular to the long sample axis was slowly increased to 1.2 T.

The actuation behavior was analyzed by measuring the MFIS of a Ni-Mn-Ga rod for different pre-loads and of the composites. For these tests, the magnetic field was perpendicular to the long sample axis and increased stepwise by steps of 0.12 T for the single crystal and the composites with the LME 10435/LME 10436 matrix and by steps of 0.24 T for the composites with the SR 8150/SD 815 B1 matrix, respectively, to a maximum field of 1.2 T. To measure the magnetic field induced strain (MFIS) of the Ni-Mn-Ga rods, the position of the glass rod was lifted after every increase of the magnetic field until the selected pre-load, applied prior to the application of the magnetic field, was regained. For the composites, the elongation was determined after achieving quasi-static conditions, until full stress relaxation of the specimens (10 min for the epoxy system LME 10435/LME 10436 and 140 min for the system SR 8150/SD 815 B1). This was necessary since the epoxy resins were viscoelastic at room temperature.

The stress-strain properties of the two epoxy systems used for the matrix were determined by tensile tests carried out on dog-bone specimens with a gage length of 25 mm. The samples were prepared by casting the resins in a silicon mold and curing them at room temperature for the same time as for the Ni-Mn-Ga composites. Quasi-static tests of the tensile epoxy samples were performed on an electromechanical testing machine from Walter+Bai Ag, Switzerland, equipped with a 50 N load cell and extensometers (the cross-head speeds selected for the tests with the two epoxy systems were 0.11 mm/min and 0.0026 mm/min for the LME 10435/LME 10436 and the SR 8150/SD 815 B1, respectively).

3. Magneto-mechanical material model for MSMA

The martensitic phases of the Ni-Mn-Ga MSMA have a tetragonal or near tetragonal unit cell with two long axes, a, and one short axis, c. This structure can, as shown in Fig. 1, be arranged in three different orientations, resulting in three possible variants which can morph into another by twinning [20]. Additionally, Ni-Mn-Ga is ferromagnetic with a high magnetic anisotropy and its magnetic easy axis aligned to the short crystallographic axis. Thus, when exposed to an external magnetic field, the variants start to re-orient by twinning so as to align the magnetic easy axis along the direction of the magnetic field, Fig. 2 (a). Similarly, twinning can also be induced by applying a mechanical force in the adequate direction, Fig. 2 (b). This deformation mechanism results in inelastic magnetic field or stress induced strains.

3.1. Mechanical behavior

The twinning planes in the two-variant single crystal specimens used in this work are always oriented 45 degrees respect of the x and y axis and the pseudo-elastic deformations are restricted to the xy plane. For these reasons, the twinning deformation was taken into account by a two dimensional Tresca yield condition which can be expressed as:

$$\phi(\sigma_{\mathrm{x}}, \sigma_{\mathrm{x}}, \tau_{\mathrm{xy}}) = (\sigma_I - \sigma_{II}) - \sigma_o = 0 \tag{1}$$

where ϕ is a limit function, σ_I and σ_{II} stand for the principal stresses in the xy plane and σ_o is the shear stress which triggers the twin motion. Assuming that the single crystal is initially in variant 1, the material deforms elastically when $\phi < 0$. However, the twining process to transform the variant 1 into variant 2 is triggered when $\phi \geq 0$ and $\sigma_x \geq \sigma_y$.

The martensitic variants evolve during twin motion from one to the other according to:

$$V_1 + V_2 = 1 \tag{2}$$

$$\dot{V}_1 = -\dot{V}_2 = \frac{\dot{\epsilon}_{eqtw}}{\epsilon_L} \tag{3}$$

where V_1 and V_2 are the volume fraction of variant 1 and 2, respectively. ϵ_L is the maximum twinning deformation and $\dot{\epsilon}_{eqtw}$ is the equivalent twinning strain rate:

$$\dot{\epsilon}_{eqtw} = \frac{\dot{\epsilon}_I - \dot{\epsilon}_{II}}{2} \tag{4}$$

with $\dot{\epsilon}_I$ and $\dot{\epsilon}_{II}$ being the principal twinning strain rates. Thus, the twinning deformation in the single crystal is complete when all the martensite in variant 1 is transformed into variant 2, corresponding to a deformation ϵ_L. Furthermore, a linear strain hardening was considered to represent the increment in the stresses upon twining as

$$\sigma_o = \sigma_{oi} + \frac{\epsilon_{eqtw}}{\epsilon_L}(\sigma_{of} - \sigma_{oi}) \tag{5}$$

where σ_{oi} and σ_{oif} are the elastic deformations for stresses below the initial twinning stress and above the final twinning stress,respectively. On the other hand, are assumed to recover during unloading (Fig. 5). The constitutive equations proposed to simulate the deformation mechanisms caused by twinning of the single crystals were integrated through a backward-Euler algorithm, assuming an associative flow.

3.2. Magnetic field induced stress

An externally applied magnetic field along the direction y, $\mathbf{B} = \mathrm{B}_y \mathbf{u}_y$, transforms the single crystal from variant 1 into variant 2 by twinning, with the subsequent elongation in the direction x (Fig. 2). Alternatively, this deformation can be obtained by applying a tensile stress along x, $\boldsymbol{\sigma}_{mag} = \sigma_{mag}\mathbf{u}_x$. Thus, the mechanical effect produced by the applied magnetic field in y direction was introduced in the constitutive model with a magnetic field induced stress acting in the direction x. It has been experimentally observed that the magnetic field induced stress is often approximated as a sigmoid function of the externally applied field [31]. Thus, the magnetic field induced stress was incorporated in the material model with the following function: :

$$\sigma_{mag} = a\left\{1 - \exp\left[-(k\mathrm{B}_y)^d\right]\right\} \tag{6}$$

where the parameters a, d and k can be obtained from fitting to the experimental stress-magnetic field measurements.

4. Numerical model

The above proposed material model was implemented in a commercial finite element code (Abaqus, [32]) through a user material model (UMAT). Since the finite element software Abaqus does not offer the possibility of coupled magneto-mechanical calculations, and as all calculations are isothermal, the temperature variable was used to simulate the magnetic field applied along the direction y (which produces an elongation along x). The details of the numerical implementation into the finite element code can be found in the Appendix. The implemented material behavior was tested in a single element model representing a single crystal subjected to uniaxial compression (applied by the displacement of corresponding face of the model) and magnetic loads. The numerical model of the composite specimens took explicitly into account the presence of both material phases and the geometry of the tested samples. One eighth of the composite samples were represented and symmetric boundary conditions were applied in the xz, xy and yz planes (Fig. 6). The geometric models of the samples were discretized with quadratic brick elements (C3D20 in Abaqus). The matrix was simulated with a linear elastic material and a perfect interface with the Ni-Mn-Ga rods was considered. The secant tensile moduli were calculated from deployed linear fit of the curves up to a deformation corresponding to the maximum MFIS. In doing so, a secant modulus of 2.5 MPa for the epoxy system LME 10435/LME 10436 and 9.0 MPa for the epoxy system SR 8150/SD 815 B1, respectively, were obtained.The simulations of the

MFIS induced by the incremental application of a magnetic field up to 1.3 T in direction y were carried out in Abaqus/Standard.

5. Results and discussion

5.1. Properties of MSMA for FE model calibration

The experimental stress-strain curves of one typical single crystal are presented in Fig. 7. The experimental data showed that the specimen deformed predominantly elastically for stresses below the initial (about 0.8 MPa) and above the final (about 2.1 MPa) twinning stress. For intermediate stress levels, stress induced twinning took place, transforming the microstructure from the long sample state (variant 2) to the short sample state (variant 1) with a maximum stress induced compression of 5.3 %. Upon unloading, the single crystal recovered the elastic deformation. The modulus obtained from the unloading branch of the curve was much higher than that from loading below the initial twinning stress. Furthermore, the transition between the elastic and twinning deformation was smooth. These facts indicate that twinning took place to a small extent even below the initial twinning stress and above the final twinning stress. Such stress-strain behavior is typical for MSMA [3, 16, 33, 31]. The developed material model (with a magnetic force of zero and a Young's modulus determined from the unloading branch) was able to adequately fit the experimental stress-strain curve. The noticeable differences observed at the beginning and the end of the twinning resulted from the simplicity of the model, Fig. 5.

As shown in Fig. 7 (b), the compressive behavior of the different single crystals differed considerably from crystal to crystal. In order to allow a description of the mechanical behavior of the four single crystals embedded in the epoxy matrix with only one set of parameters, single crystals with similar stress-strain curve were classified in four different groups to prepare the four composites specimens studied in this work. Groups 1 and 2 were employed to manufacture specimens with the epoxy system LME 10435/LME 10436 with 34% and 13% volume fraction, respectively. Groups 3 and 4 were embedded in SR 8150/SD 815 B1 with volumes fractions of 34 % and 13 %. The different mechanical behavior of the rods was then included in the model by adjusting the final twinning stress and strain, to correspond to a given group of 4 MSMA rods. All input parameters used in the model to describe the magneto-mechanical behavior are given in Table 1.

The stress induced in the single crystal by an applied magnetic field was incorporated into the material model as a fit of the experimental stress-magnetic field curve using equation 5, as shown in Fig. 8 and Table 1. The stress plateau of 2.4 MPa at high magnetic fields corresponds to the macroscopic maximum

force effect of the magnetic field. Therefore, the maximum stress induced by the external magnetic field is slightly higher that the final twinning stress. This fact implies that all the twins in the specimen can be activated by applying a magnetic field over 1 T [34]. Thus, a full reorientation of the martensitic variants is expected by the application of a magnetic field.

The experimental MFIS together with the numerical predictions of a Ni-Mn-Ga single crystal for five different pre-loads are shown in Fig. 9. No noticeable MFIS was observed for small magnetic fields (below 0.22 T) since the stress induced by the field was not sufficient to induce twin boundary motion. With increasing magnetic field, more and more twinning took place transforming the microstructure from the short sample state (variant 1) to the long sample state (variant 2) and resulting in an increasing MFIS. For high magnetic fields, the MFIS asymptotically reached a plateau indicating that no further twin boundary motion was possible. This asymptotic increase was cut off at about 0.7 T if no pre-load was applied to the sample indicating that the crystal was fully transformed. With increasing pre-load along the long sample axis and perpendicular to the field, the MFIS rise was shifted to higher magnetic fields and the maximum MFIS decreased from 5.3 % at no pre-load to 0.2 % at 2.4 MPa. Thus, for no pre-load, the MFIS approximately corresponds to the final twinning strain obtained in the compression test. However, the MFIS is almost blocked for a pre-load corresponding to the maximum force effect of the magnetic field.

This model implemented into the finite element code was able to adequately describe the magneto-mechanical behavior of the Ni-Mn-Ga single crystal. The numerical model captured the shift in the beginning of the MFIS to higher magnetic fields with increasing pre-load, the non-linear evolution of the MFIS and the decreasing maximum MFIS with increasing pre-load. The deviations of the predicted actuation behaviour from the experimental one can be attributed to the simplifications in the simulated stress-strain curve.

5.2. Actuation behaviour of Ni-Mn-Ga single crystal-epoxy matrix composites

The magnetic responses of the four Ni-Mn-Ga single crystal-epoxy matrix composites are shown in Fig. 10. Similarly to the case of the bulk MSMA samples, no MFIS was detected for magnetic fields smaller than the field necessary to induce twinning. The critical magnetic field, which initiated the MFIS, was approximately 0.22 T. This value, observed for the four composites specimens, corresponded to the critical field observed for the single crystalline sample with no pre-load. This indicates that no considerable residual stresses were developed in the composite while curing at room temperature. After the onset, the evolution of the MFIS with the applied magnetic field was almost linear in the

four specimens up to 0.7 T. The slope of the magneto-mechanical response in this region depended on the matrix stiffness and on the volumetric fraction of Ni-Mn-Ga. The saturation of the MFIS, on the other hand, was reached at the same time in all composites for magnetic fields larger than about 0.9 T. Regarding the maximum MFIS, the Ni-Mn-Ga composite with the epoxy system LME 10435/LME 10436 as matrix and a Ni-Mn-Ga volume fraction of 34 % exhibited about the same value as the four Ni-Mn-Ga single crystals used to prepare the composite, i.e. reached the maximum strain expected to 5.3 %. For the other three composites, the compressive forces that built up in the strained matrix were high enough to partly hinder twinning. The maximum actuation strain of Ni-Mn-Ga single crystal composites can hence be regulated by changing the Ni-Mn-Ga volume fraction and/or the matrix stiffness.

The numerical predictions of the magnetic field induced strain (measured from the averaged displacement of all the nodes of the upper face of the composite) for an increasing magnetic field, Fig. 10, were able to reproduce the onset of twinning, the increase of the MFIS and the saturation of the MFIS for magnetic fields higher than about 0.9 T. The maximum strains obtained from the simulations are in good agreement with the experiments for the four composites specimens studied. The small deviations between the experiments and the simulations are probably due to the assumptions of simplified stress-strain behaviour and of the same stress-magnetic field curve for all the single crystals in each specimen.

The contour plots in Fig. 11 illustrate the numerical predictions for the volumetric fraction of variant 2 evolved by twin boundary motion from variant 1 at a magnetic field of 1.3 T for all four Ni-Mn-Ga single crystal composites. While the single crystals embedded with a Ni-Mn-Ga volume fraction of 34 vol.% in the epoxy system LME 10435/LME 10436 transform almost completely into variant 2, the transformation is not complete for the other three composites even for high magnetic fields. Thus, the forces developed in the matrix SR 8150/SD 815 B1 and LME 10435/LME 10436 (for a Ni-Mn-Ga volume fraction of 13 vol.%) are high enough to partly hinder twinning. Furthermore, the evolution of variant 2 is not homogeneous along the Ni-Mn-Ga single crystal. At the surface, less stresses build up in the matrix allowing the crystals to transform more extensively close to the free surface.

Besides the numerical simulations, the maximum MFIS can be calculated using an analytical isostrain model, as proposed by Gans et al. [16]. Assuming force balance between the force in the MSMA and the matrix if an external magnetic field is applied to the composite sample and neglecting elastic deformations of the MSMA, the MFIS of the composite is given by:

$$\epsilon_{MFIS,comp} = \frac{E_{MSMA}\epsilon_{MFIS,MSMA}}{E_{matrix}\left(\frac{1-V_{MSMA}}{V_{MSMA}}\right) + E_{MSMA}} \quad (7)$$

where E_{MSMA} is the Young's modulus of the MSMA elements during twinning, E_{matrix} the Young's modulus of the polymer matrix, $\epsilon_{MFIS,MSMA}$ the MFIS of the non-embedded MSMA element and V_{MSMA} the volumetric fraction of the MSMA elements in the composite.

The comparison of the experimental maximum MFIS values of the four composites with the results of the FE simulations and the isostrain model is presented in Fig. 12. Agreement with the FE simulation is very satisfactory, and better than with the analytical isostrain model.

The maximum MFIS obtained from the FE simulations of Ni-Mn-Ga composites with different volume fractions and matrix stiffness is shown in Fig. 13 together with the predictions of the isostrain model. Both models indicate the same trend, that low matrix stiffness is necessary to avoid the need for a large volume fraction of single crystal rods. The isostrain model seems to underestimate the maximum MFIS of composites for all Ni-Mn-Ga volume fractions and matrix stiffness. This is expected since the analytical isostrain model does not take into account the geometry of the composite, the shape and distribution of the Ni-Mn-Ga single crystals in the matrix and inhomogeneous strains in the composite. In particular, at low volume fraction MSMA, around 5 to 10 %, with a matrix modulus below 5 MPa, strains already above 2.5 % can be easily attained.

6. Conclusions

Ni-Mn-Ga single crystal-epoxy matrix composites were successfully produced and their magneto-mechanical behavior was characterized. Depending on the Ni-Mn-Ga volume fraction and matrix stiffness, twinning was partially hindered by stresses developing in the matrix resulting in a reduction of the maximum magnetic field induced strain. Nonetheless, large actuation strains could be obtained with the low modulus matrix already with realistic volume fractions of MSMA rods. In parallel, FE simulations taking into account the magneto-mechanical behavior of the MSMA rods and the elastic behavior of the epoxy resins were carried out to reproduce the behavior of MSMA unidirectional composites. Numerical models showed very good agreement with experimental results for the four types of composites produced, and thus provided a tool to predict the behavior of composites, as a function of volume fraction, geometrical arrangement, matrix and MSMA properties, which is more precise than the simple analytical iso-strain model. These models also showed that in order to

reach large strains, the matrix should be selected as a material with low elastic modulus, around 5MPa. The epoxy analyzed in the experimental work was a useful model system, but matrices exhibiting less strain sensitivity such as silicone would be better suited to reach high frequency actuation.

Acknowledgment

This work is supported by the Swiss National Science Foundation under the National Research Programme NRP 62 n° 406240-126120. We would like to thank Prof. Peter Müllner from Boise State University for his advice on interpretation and simulation of magnetic field induced forces in Ni-Mn-Ga.

Appendix

Under the small deformation assumption the total strain increment ($\Delta\boldsymbol{\epsilon}$) can be obtained as the sum of the elastic ($\Delta\boldsymbol{\epsilon}_e$) and inelastic ($\Delta\boldsymbol{\epsilon}_{tw}$) increments.

$$\Delta\boldsymbol{\epsilon} = \Delta\boldsymbol{\epsilon}_e + \Delta\boldsymbol{\epsilon}_{tw} \tag{8}$$

The constitutive equations were integrated in the numerical model through a backward-Euler implicit method (Fig. 14 a). Starting from the last converged step (t), a new strain increment ($\Delta\boldsymbol{\epsilon}$) was applied at $t + \Delta t$. An initial trial stress state ($\boldsymbol{\sigma}^{(trial)}$) was calculated assuming a fully elastic behavior

$$\boldsymbol{\sigma}^{(trial)} = \boldsymbol{\sigma}^{(t)} + \Delta\boldsymbol{\sigma}^{(trial)} = \boldsymbol{\sigma}^{(t)} + \mathbf{C}\Delta\boldsymbol{\epsilon}^{(t+\Delta t)} + \Delta\boldsymbol{\sigma}_{mag}{}^{(t+\Delta t)} \tag{9}$$

with $\mathbf{C}$ the matrix of elastic constants. Additionally, the effect of the magnetic field was introduced in the numerical model as an additional stress tensor ($\boldsymbol{\sigma}_{mag}$) evolving with the applied magnetic field as

$$\Delta\boldsymbol{\sigma}_{mag} = \frac{\partial\boldsymbol{\sigma}_{mag}}{\partial \mathrm{B}_y}\Delta \mathrm{B}_y \tag{10}$$

where B_y stands for the magnetic field in direction y. The limit function is verified at the trial state. Assuming that the crystal is in variant 1, if $\phi(\boldsymbol{\sigma}^{(trial)}) < 0$ the step is considered fully elastic and the stresses and strains are updated.

$$\boldsymbol{\sigma}^{(t+\Delta t)} = \boldsymbol{\sigma}^{(t)} + \mathbf{C}\Delta\boldsymbol{\epsilon}^{(t+\Delta t)} + \Delta\boldsymbol{\sigma}_{mag}{}^{(t+\Delta t)} \tag{11}$$

$$\boldsymbol{\epsilon}^{(t+\Delta t)} = \boldsymbol{\epsilon}^{(t)} + \Delta\boldsymbol{\epsilon}^{(t+\Delta t)} \tag{12}$$

If $\phi(\boldsymbol{\sigma}^{(trial)}) \geq 0$ and $\sigma_x \geq \sigma_y$ the trial state is in the inelastic region and the stresses should return to the yield surface. The backward-Euler method ensure

that the return is normal to the yield surface. For an associative yield flow, this return algorithm is defined by the condition:

$$\boldsymbol{\sigma}^{(t+\Delta t)} - (\boldsymbol{\sigma}^{(trial)} - \Delta\lambda \mathbf{C}\mathbf{a}^{(t+\Delta t)}) = 0 \tag{13}$$

where $\mathbf{a}^{(t+\Delta t)} = \partial\phi/\partial\boldsymbol{\sigma}^{(t+\Delta t)}$ is the normal to the yield surface at the returning point and $\Delta\lambda$ is a inelastic multiplier. Once the solution in the stresses was found, the elastic and the twinning strains ($\boldsymbol{\epsilon}_e$ and $\boldsymbol{\epsilon}_{tw}$, respectively)were updated.

$$\boldsymbol{\epsilon}_e{}^{(t+\Delta t)} = \boldsymbol{\epsilon}_e{}^{(t)} + (\Delta\boldsymbol{\epsilon}_e{}^{(t+\Delta t)} - \Delta\lambda \mathbf{a}^{(t+\Delta t)}) \tag{14}$$

$$\boldsymbol{\epsilon}_{tw}{}^{(t+\Delta t)} = \boldsymbol{\epsilon}_{tw}{}^{(t)} + \Delta\lambda \mathbf{a}^{(t+\Delta t)} \tag{15}$$

Finally, the equivalent twinning strain and the variant state were updated in the actual step through Eqs. 3 and 4. When $\epsilon_{eqtw} = \epsilon_L$ the single crystal is fully transformed into variant 2, the maximum twinning deformation is achieved ($\boldsymbol{\epsilon}_{tw} = \epsilon_L \mathbf{u}_x - \epsilon_L \mathbf{u}_y$)and the elastic behavior is recovered (Fig. 14 b). The elastic behavior is recovered at this point and the transformation back into variant 1 is then triggered when $\phi(\boldsymbol{\sigma}) \geq 0$ and $\sigma_x \leq \sigma_y$.

References

[1] C. Lexcellent, Shape-memory Alloys Handbook, John Wiley & Sons, 2013.

[2] V. Michaud, Can shape memory alloy composites be smart?, Scripta Materialia 50 (2) (2004) 249–253.

[3] A. Sozinov, A. A. Likhachev, N. Lanska, K. Ullakko, Giant magnetic-field-induced strain in NiMnGa seven-layered martensitic phase, Applied Physics Letters 80 (10) (2002) 1746–1748.

[4] N. Scheerbaum, D. Hinz, O. Gutfleisch, K. H. Muller, L. Schultz, Textured polymer bonded composites with Ni-Mn-Ga magnetic shape memory particles, Acta Materialia 55 (8) (2007) 2707–2713.

[5] K. Ullakko, Magnetically controlled shape memory alloys: a new class of actuator materials, Journal of materials Engineering and Performance 5 (3) (1996) 405–409.

[6] M. Kohl, D. Brugger, M. Ohtsuka, T. Takagi, A novel actuation mechanism on the basis of ferromagnetic SMA thin films, Sensors and Actuators A: Physical 114 (2) (2004) 445–450.

[7] J. Feuchtwanger, S. Michael, J. Juang, D. Bono, R. C. OHandley, S. M. Allen, C. Jenkins, J. Goldie, A. Berkowitz, Energy absorption in Ni-Mn-Ga-polymer composites, Journal of Applied Physics 93 (10) (2003) 8528–8530.

[8] M. Lahelin, I. Aaltio, O. Heczko, O. Söderberg, Y.Ge, B. Löfgren, S.-P. Hannula, J. Seppälä, Dma testing of NiMnGa/polymer composites, Composites Part A: Applied Science and Manufacturing 40 (2009) 125–129.

[9] D. C. Dunand, P. Müllner, Size effects on magnetic actuation in Ni-Mn-Ga shape-memory alloys, Advanced Materials 23 (2) (2011) 216–232.

[10] S. Glock, X. X. Zhang, N. J. Kucza, P. Müllner, V. Michaud, Structural, physical and damping properties of melt-spun Ni-Mn-Ga wire-epoxy composites, Composites Part A: Applied Science and Manufacturing 63 (2014) 68–75.

[11] S. Glock, E. Spārniņš, Y. Leterrier, V. Michaud, Effect of annealing and simulation on the strength of melt-spun nimnga fibres and their adhesion to epoxy, International Journal of Adhesion and Adhesives 55 (2014) 89–94.

[12] B. Tian, F. Chen, Y. X. Tong, L. Li, Y. F. Zheng, Y. Liu, The orientation dependence of transformation strain of NiMnGa polycrystalline alloy and its composite with epoxy resin, Journal of Alloys and Compounds 505 (2010) 680–684.

[13] S. P. Hannula, I. Aaltio, Y. Ge, M. Lahelin, Söderberg, Processing and properties of Ni-Mn-Ga magnetic shape memory alloy based hybrid materials, Current Applied Physics 12 (2012) S63–S67.

[14] X. Sun, C. Xie, Effect of volume fraction of NiMnGa powders on magnetic-field-induced strain in NiMnGa/polymer composites, Advanced Materials Research (2011) 387–390.

[15] S. Kauffmann-Weiss, N. Scheerbaum, J. Liu, H. Klauss, L. Schultz, E. Mäder, R. Häßler, G. Heinrich, O. Gutfleisch, Reversible magnetic field induced strain in Ni2MnGa-polymer-composites, Advanced Engineering Materials 14 (2012) 20–27.

[16] E. Gans, G. P. Carman, Cyclic actuation of Ni-Mn-Ga composites, Journal of Applied Physics 99 (8) (2006) 084905(1)–084905(4).

[17] B. Cox, Q. Yang, In quest of virtual tests for structural composites, Science 314 (2006) 1102–1107.

[18] J. LLorca, C. González, J. M. Molina-Aldareguía, J. Segurado, R. Seltzer, F. Sket, M. Rodríguez, S. Sádaba, R. M. noz, L. P. Canal, Multiscale modeling of composite materials: a roadmap towards virtual testing, Advanced Materials 23 (44) (2011) 5130–5147.

[19] L. Hirsinger, C. Lexcellent, Modelling detwinning of martensite platelets under magnetic and (or) stress actions on Ni-Mn-Ga alloys, Journal of Magnetism and Magnetic Materials 254 (2003) 275–277.

[20] B. Kiefer, D. C. Lagoudas, Magnetic field-induced martensitic variant reorientation in magnetic shape memory alloys, Philosophical Magazine 85 (33-35) (2005) 4289–4329.

[21] B. Kiefer, D. C. Lagoudas, Modeling of the variant reorientation in magnetic shape-memory alloys under complex magnetomechanical loading, Materials Science and Engineering: A 481 (2008) 339–342.

[22] A. A. Likhachev, K. Ullakko, Magnetic-field-controlled twin boundaries motion and giant magneto-mechanical effects in Ni-Mn-Ga shape memory alloy, Physics Letters A 275 (1) (2000) 142–151.

[23] A. A. Likhachev, A. Sozinov, K. Ullakko, Different modeling concepts of magnetic shape memory and their comparison with some experimental results obtained in Ni-Mn-Ga, Materials Science and Engineering a-Structural Materials Properties Microstructure and Processing 378 (1-2) (2004) 513–518.

[24] B. Kiefer, H. E. Karaca, D. C. Lagoudas, I. Karaman, Characterization and modeling of the magnetic field-induced strain and work output in Ni2MnGa magnetic shape memory alloys, Journal of Magnetism and Magnetic Materials 312 (1) (2007) 164–175.

[25] B. Krevet, M. Kohl, P. M. S. Seelecke, Magnetization-and strain-dependent free energy model for FEM simulation of magnetic shape memory alloys, The European Physical Journal Special Topics 158 (1) (2008) 205–211.

[26] K. Haldar, B. Kiefer, D. C. Lagoudas, Finite element analysis of the demagnetization effect and stress inhomogeneities in magnetic shape memory alloy samples, Philosophical Magazine 91 (32) (2011) 4126–4157.

[27] J. Wang, P. Steinmann, Finite element simulation of the magneto-mechanical response of a magnetic shape memory alloy sample, Philosophical Magazine 93 (20) (2013) 2630–2653.

[28] J. Lubliner, F. Auricchio, Generalized plasticity and shape memory alloys, International Journal of Solids and Structures 33 (7) (1996) 991–1003.

[29] F. Auricchio, R. L. Taylor, Shape-memory alloys: modelling and numerical simulations of the finite-strain superelastic behavior, Computer Methods in Applied Mechanics and Engineering 143 (1) (1997) 175–194.

[30] M. A. Qidwai, D. C. Lagoudas, Numerical implementation of a shape memory alloy thermomechanical constitutive model using return mapping algorithms, International Journal for Numerical Methods in Engineering 47 (6) (2000) 1123–1168.

[31] V. A. Chernenko, V. A. L'vov, P. Müller, G. Kostorz, T. Takagi, Magnetic-field-induced superelasticity of ferromagnetic thermoelastic martensites: Experiment and modeling, Physical Review B 69 (13) (2004) 134410(1)–134410(8).

[32] Abaqus, User Manual, version 6.11, Abaqus Inc., 2012.

[33] L. Straka, N. Lanska, K. Ullakko, A. Sozinov, Twin microstructure dependent mechanical response in Ni-Mn-Ga single crystals, Applied Physics Letters 96 (13) (2010) 131903(1)–131903(3).

[34] A. Sozinov, A. A. Likhachev, K. Ullakko, Crystal structures and magnetic anisotropy properties of Ni-Mn-Ga martensitic phases with giant magnetic-field-induced strain, Ieee Transactions on Magnetics 38 (5) (2002) 2814–2816.

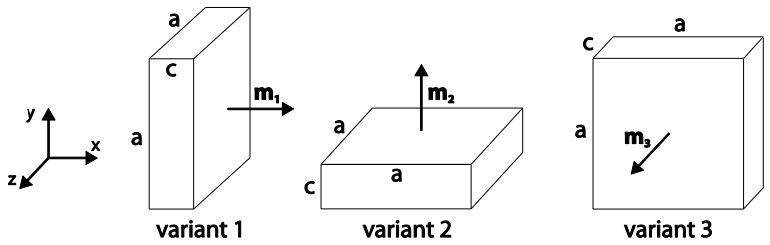

Figure 1: Possible martensitic variants in Ni-Mn-Ga magnetic shape memory alloys.

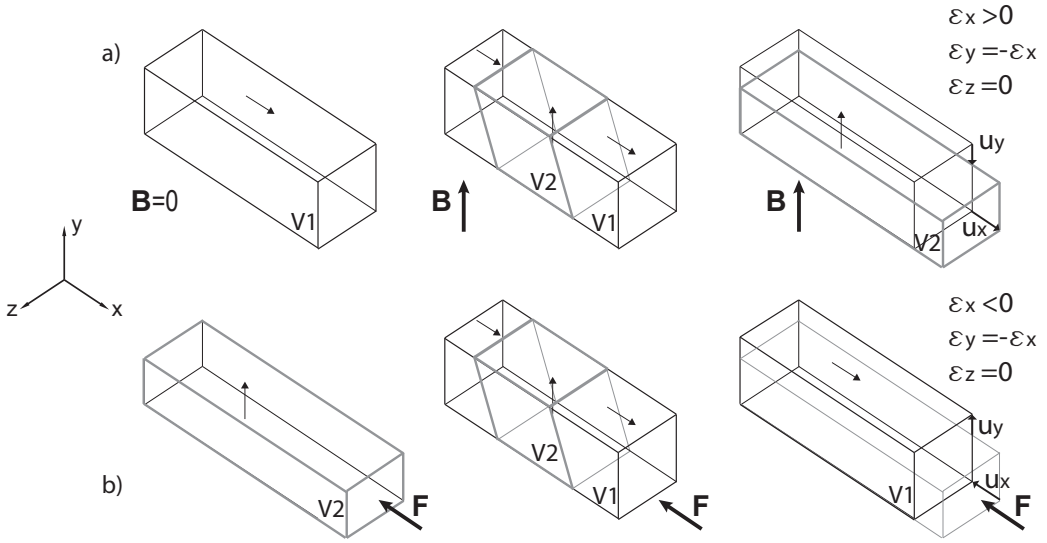

Figure 2: Schematic of the deformation in a two-variant Ni-Mn-Ga single crystal upon the application of (a) an external magnetic field and (b) a mechanical load.

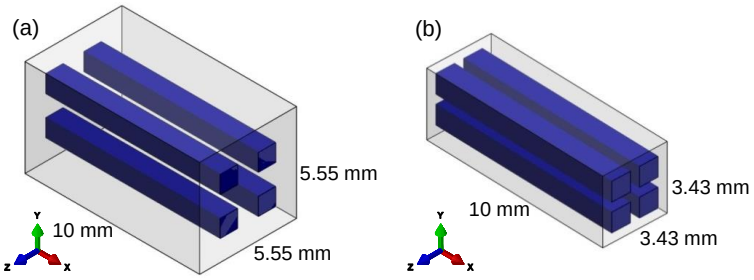

Figure 3: Schematic of the Ni-Mn-Ga single crystal-epoxy matrix composites with a Ni-Mn-Ga volumetric fraction of 13 vol. % (a) and 34 vol. % (b).

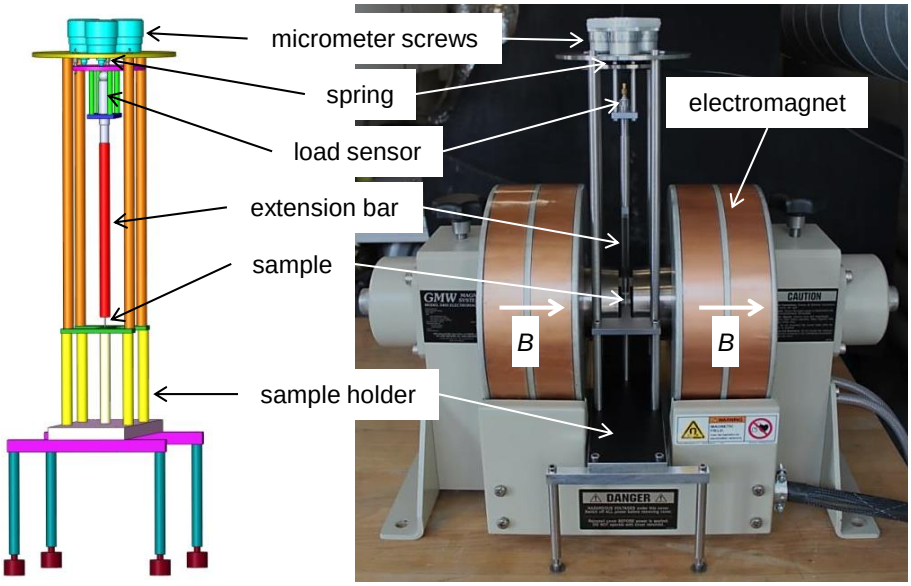

Figure 4: Home-made set-up used to characterize the magneto-mechanical behavior of Ni-Mn-Ga single crystalline rods and Ni-Mn-Ga epoxy matrix composites.

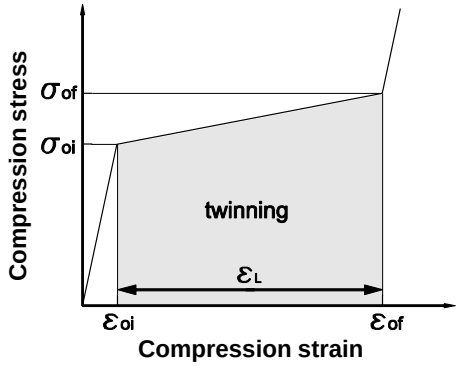

Figure 5: Schematic of the stress-strain curve for a uniaxial compression test.

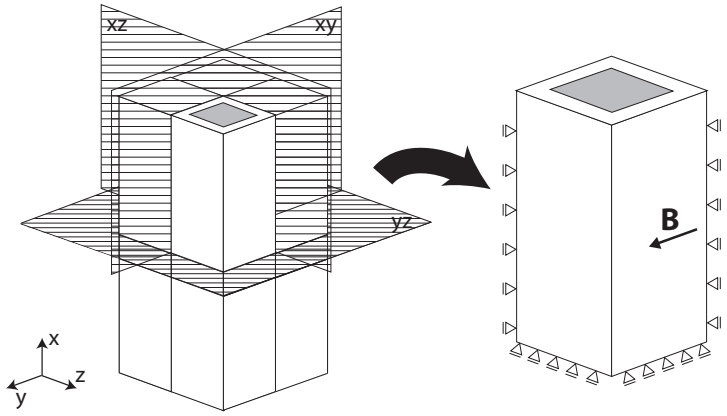

Figure 6: Schematic of numerical model and the boundary conditions for the simulation of the actuation of Ni-Mn-Ga composites.

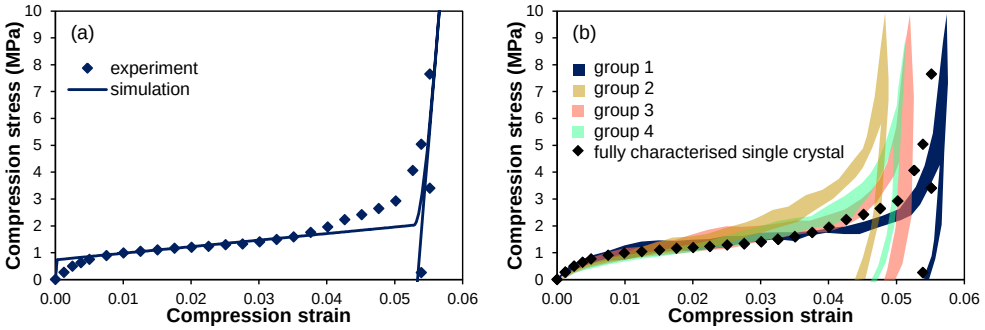

Figure 7: (a) Compressive stress-strain curve of a Ni-Mn-Ga single crystal and (b) Differences of in each case four single crystals grouped to prepare the different composites. The dots correspond to one single crystal that was used as the reference for full characterization.

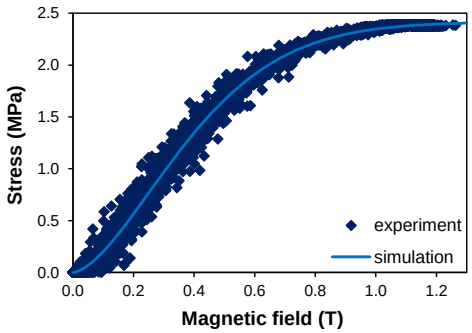

Figure 8: Magnetic field induced stress of a Ni-Mn-Ga single crystal.

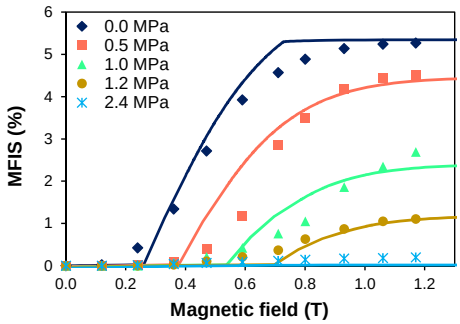

Figure 9: Experimentally measured and simulated magnetic field induced strains of a Ni-Mn-Ga single crystal for different pre-loads.

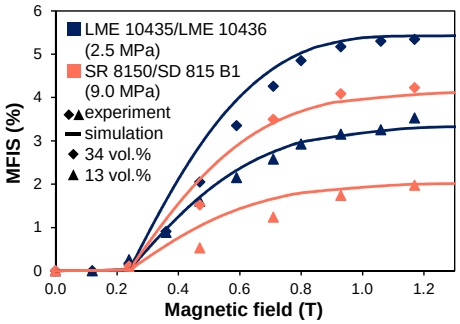

Figure 10: Magnetic field induced strains of the Ni-Mn-Ga single crystal epoxy matrix composites.

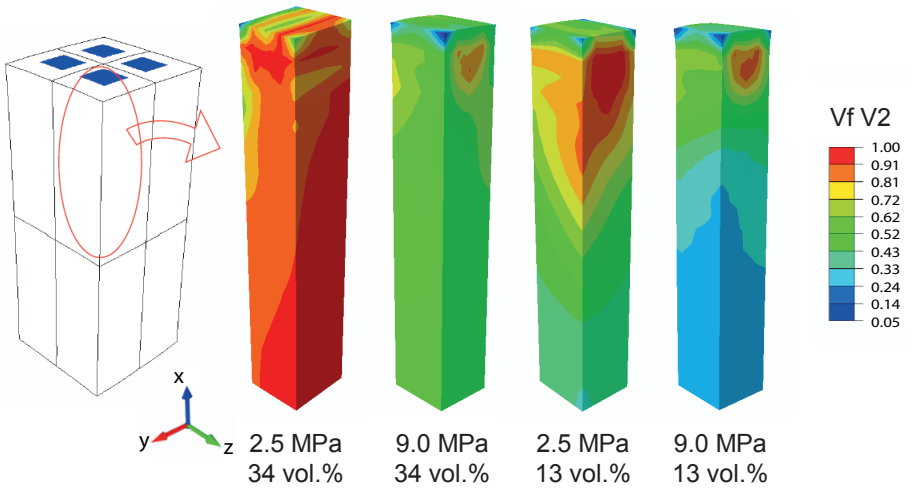

Figure 11: Contour plots of the volumetric fraction of variant 2 evolved by twinning from variant 1 at a magnetic field of 1.3 T for the Ni-Mn-Ga single crystals embedded in epoxy.

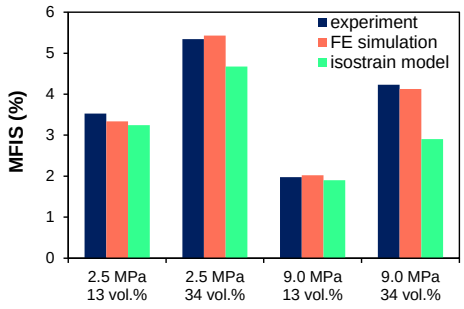

Figure 12: Comparison of the experimental maximum MFIS values of the four composites with the results of the FE simulations and the values calculated using the isostrain model

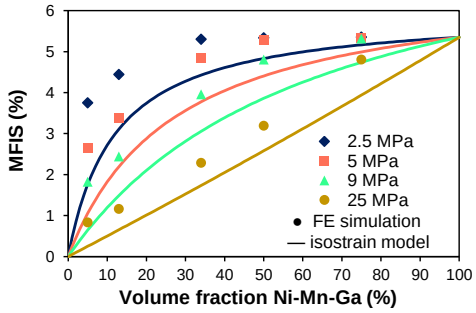

Figure 13: Influence of Ni-Mn-Ga volume fraction and matrix stiffness on the maximum MFIS according to the FE simulations and the isostrain model results. Please note that model values for are taken as the fully characterised single crystal.

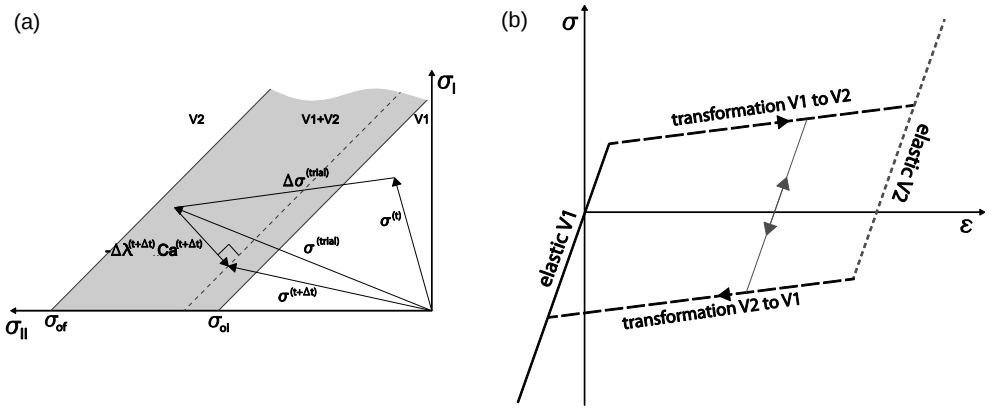

Figure 14: (a) Representation of the twinning region in the space of principal stresses 1- 2 for a two-variant single crystal initially in variant 1 and (b) Schematic of the stress-strain curves for a uniaxial tension-compression test.

Table 1: Input parameters used in the model to describe the magneto-mechanical behavior of the fully characterized single crystal (fc crystal) and the 4 groups of crystals used to prepare the composites.

crystal	E (GPa)	σ_{oi} (MPa)	σ_{of} (MPa)	ϵ_L (%)	a (MPa)	k (T^{-1})	d (-)
fc crystal			2.03	5.5			
group 1			2.62	4.9			
group 2	3.1	0.75	1.90	5.2	2.41507	2.20157	1.61276
group 3			2.50	4.7			
group 4			2.07	5.6			